Explicit Simulation of a Tropical Mesoscale Convective System

G. D. Alexander and W. R. Cotton
Colorado State University
Fort Collins, Colorado

Introduction

We have used Colorado State University's Regional Atmospheric Modeling System (RAMS) to simulate the MCS observed during the ninth flight mission of the Equatorial Mesoscale Experiment (EMEX9). Research aircraft probed EMEX9 on 2-3 February 1987. Mapes and Houze (1992) and Mapes and Houze (1993) provided a detailed view of the horizontal and vertical structure, respectively, of the ten EMEX precipitation systems. Synoptic conditions for EMEX9 are described by Bograd (1989) and Mapes (1992). EMEX9 has been two-dimensionally modelled by Wong et al. (1993) and Tao et al. (1993).

First, we discuss the synoptic situation surrounding EMEX9 and observations of the EMEX9 convective system. Second, we discuss our model setup and results of our simulation. Third, we discuss various analysis techniques which we have applied to our results. We summarize our results at the end of the paper.

Observations

EMEX9 occurred during an active period of the 1987 Australian monsoon, where "active" means that the mean 850 mb westerly wind in the region 110°-140°E, 5°-15°S exceeded 8 ms^{-1} (Webster and Houze 1991). The prevailing synoptic feature at the time of EMEX9 was a deep westerly monsoon trough extending from 500 mb to the surface which oriented itself across Arnhem Land of northern Australia and into New Guinea. A composite sounding of the EMEX9 environment, assembled using all available aircraft and synoptic data, has a convective available potential energy (CAPE) of 1484 Jkg^{-1} and a bulk Richardson number of 51, typical of multicellular convection.

The NOAA P-3, NCAR Electra, and CSIRO F-27 aircraft all penetrated EMEX9 in the hours roughly between 2100 UTC and 0100 UTC. The P-3 Doppler radar observed two separate convective lines—an initial line oriented in a west-northwest to east-southeast direction which was more than 300 km long, and a northwest to southeast oriented convective line which was about 250 km long. Maximum observed updraft strengths were on the order of 7-9 ms^{-1}.

Simulation

Setup

We initialize RAMS with the a special Australian Monsoon Experiment (AMEX) data set (1.25° grid spacing and 11 vertical levels) at 1100 UTC (2130 LST) 2 February 1987. The RAMS ISAN (ISentropic ANalysis) package interpolates this data set onto 33 isentropic level and applies the Barnes (1973) objective analysis scheme. We also include horizontally variable topography (10 minute horizontal grid spacing) and February 1987 sea surface temperature (1° horizontal grid spacing). The model's horizontal grid spacing is 24 km on Grid #1, 6 km on Grid #2 , and 1.5 km on Grid #3 (Figure 1). We use 35 vertical levels, stretched from a spacing of 100 m near the surface to 1000 m at the model top, which is at about 22 km. During the first hour of the simulation, we use only the coarsest grid. At that point, we activate the two finer grids. The timesteps are 24, 8, and 4 seconds for Grids # 1, # 2, and # 3, respectively. We use the deep convection component (as opposed to the turbulence component) of the Level 2.5w convective parameterization scheme (Weissbluth and Cotton 1993) on all grids for the first 90 minutes of the simulation. Then, it is turned off on all grids, so all convection after that point is explicitly simulated. We explicitly simulate

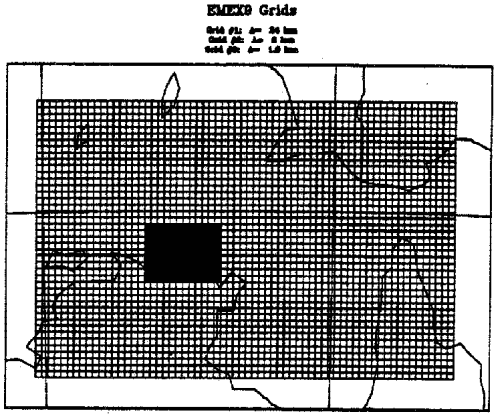

Figure 1. Grid setup for the EMEX9 simulation. Grid spacing is 24, 6, and 1.5 km on Grids #1, #2, and #3, respectively.

the convection in EMEX9 for 4.5 hours, between 1330 and 1800 UTC (the system's total lifetime was about 12 hours).

Results

The RAMS simulation captures many of the key features of EMEX9. Three-dimensional plots provide a perspective of the simulated EMEX9 convection. Figure 2, for instance, shows the 0.5 gkg^{-1} surface of condensate mixing ratio at 1400 UTC. A dramatic leading anvil stretches from east to west across the grid, with convective towers trailing behind. This convective line is forced by the collision of the westerly

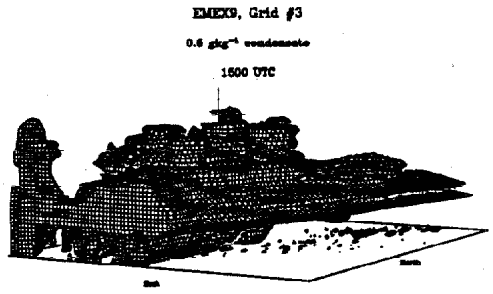

Figure 2. Three-dimensional plot of the 0.5 gkg^{-1} condensate surface on Grid #3 at 1400 UTC. Perspective is from the northeast.

monsoon flow and the southerly land-breeze flow. By 1800 UTC (not shown) the stratiform anvil extends both ahead of and behind the convection, and blankets all of Grid #3, as the convection propagates toward the northeast at 10-15 ms^{-1} along the monsoon trough.

Analysis Techniques

Conditional Sampling

We have applied conditional sampling criteria to our model results in order to identify key features of EMEX9's convective, stratiform, and intermediary regions (only the latter will be discussed here). In conditionally sampling our fine grid, we take any grid point with a rain mixing ratio of at least 0.5 gkg^{-1} at the lowest model level to be convective. If this rain mixing ratio is greater than 0 but less than 0.25 gkg^{-1} the grid point is stratiform. A grid point with a rain mixing ratio of between 0.25 and 0.50 gkg^{-1} at the lowest model level is considered to be in the intermediary region. This region is called intermediary because it is intermediate between convective and stratiform precipitation both spatially and temporally, in general (e.g., Mapes and Houze 1993).

We have evaluated mean divergence over all of Grid #3, and in the conditionally sampled intermediary region. The time series of mean divergence for all of Grid # 3 (Figure 3) has an elevated maximum in the 4-5 km range. Mapes and Houze (1993), who presented Doppler-derived vertical profiles of horizontal divergence for EMEX systems, also observed an elevated convergence maximum at 4 km or so. Mapes (1993) argues that an elevated convergence maximum is significant because it promotes upward displacements at low levels in the nearby atmosphere, thereby favoring additional convection. The mean divergence time series for the intermediary region (Figure 4) appears more chaotic, but at several times exhibits robust convergence maxima at the unusually high levels of 11-12 km.

These convergence maxima at high levels are reminiscent of the Doppler-derived vertical profiles of horizontal divergence for intermediary regions of EMEX convective systems presented by Mapes and Houze (1993), not only in their vertical location, but also in their magnitudes. Mapes and Houze attribute the convergence maximum

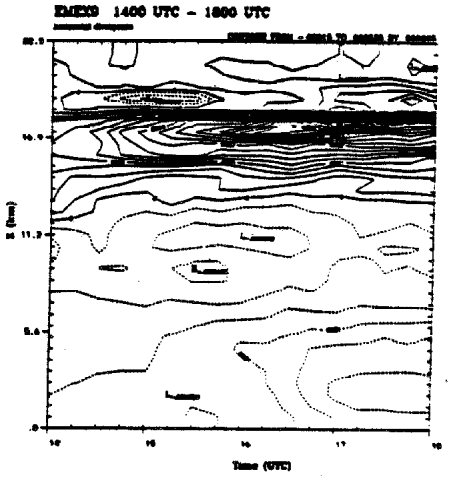

Figure 3. Time series of the vertical profile of simulated mean horizontal divergence (s^{-1}) between 1400 UTC and 1800 UTC for all regions of Grid #3.

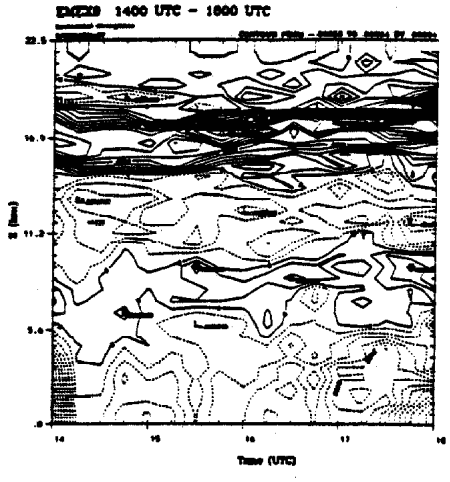

Figure 4. Time series of the vertical profile of simulated mean horizontal divergence (s^{-1}) between 1400 UTC and 1800 UTC for intermediary regions of Grid #3.

near 10 km in intermediary regions to the atmosphere's inability to instantly deal with a large amount of mass ascending in convective cells. As a result, the convective cells must detrain their mass flux over a deep layer of the upper troposphere, much of it below its level of neutral buoyancy, with the resulting deep slab of cloudy outflow collapsing and spreading out at its level of neutral buoyancy.

Lagrangian Particle Dispersion Modelling

We have applied the RAMS Lagrangian Particle Dispersion Model (LPDM), which simulates the motion of tracers under the influence of atmospheric flow, to EMEX9. After the initial RAMS simulation, we can apply the RAMS LPDM in any number of ways. For instance, in Figure 5 we show 120-minute (1430-1630 UTC) system-relative forward trajectories for particles that the LPDM releases at 1 km.

Particles released at 1 km move in a front-to-rear direction. The vertical displacement of these trajectories occurs along a west-northwest to east-southeast oriented line. In two convective cells, this 1 km tracer ascends to the 14-16 km level. Most particles which do not get drawn into these convective cells do not ascend much higher than 5 km.

We are able to compute the ambient value along a particle's trajectory of any quantity which can be computed from the model's output variables. For instance, we have evaluated the vertical gradient $\left(\frac{\partial}{\partial z}\right)$ of terms in the nonhydrostatic

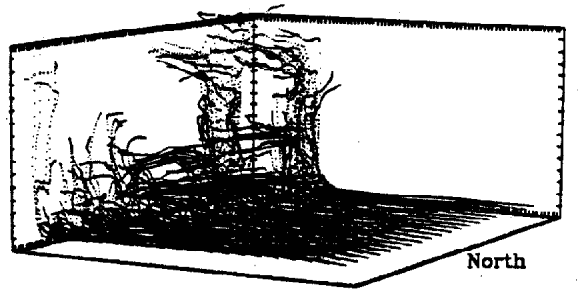

Figure 5. System-relative trajectories of particles released at 1 km. On Grid #3, 400 evenly-spaced particles are released at 1430 UTC. The perspective is from the northeast. Tick marks along the horizontal axes are at 1.5 km intervals (the grid spacing on Grid #3). Tick marks along the vertical axis are at 1 km intervals, from the surface to 16 km.

pressure perturbation equation in order to ascertain which physical effects are responsible for pressure-gradient-induced ascent in typical front-to-rear ascending trajectories. The nonhydrostatic pressure perturbation equation may be written in the approximate form

$$-\theta_0 \nabla^2 \pi' = \left(\frac{\partial u}{\partial x}\right)^2 + \left(\frac{\partial v}{\partial y}\right)^2 + \left(\frac{\partial w}{\partial z}\right)^2 + 2\frac{\partial v}{\partial x}\frac{\partial v}{\partial y} + 2\frac{\partial w}{\partial x}\frac{\partial u}{\partial z} + 2\frac{\partial w}{\partial y}\frac{\partial y}{\partial z} + \frac{\partial}{\partial z}\left(\frac{\theta_v'}{\theta_0} - r_w'\right)g \quad (1)$$

where π' is the perturbation Exner function.

Terms 1, 2, and 3 on the right-hand side are fluid extension terms. Term 4 is a fluid shear term. Terms 5 and 6 indicate that there will be a positive (negative) pressure perturbation on the upshear (downshear) flank of an updraft. Term 7 indicates that there will be a positive (negative) pressure perturbation in regions where buoyancy is locally decreasing (increasing) with height.

The qualitative behavior of $-\nabla^2 \pi'$ may be found by noting that for a function consisting of a narrow band of Fourier components, the Laplacian of the function is negatively proportional to the function itself. That is, $-\nabla^2 \pi' \propto \pi'$.

We have evaluated the value of the vertical gradient of the perturbation Exner function and the values of the *vertical gradient* of the terms on the right hand side of (1) along two 120-minute (1430-1630 UTC) system-relative front-to-rear ascending trajectories for EMEX9. Both trajectories start at 1 km. One ascends to about 6 km. The other ascends to about 14 km. Our computations show that the vertical gradient of the buoyancy gradient term is an order of magnitude larger than any of the other terms for these particular front-to-rear ascending system-relative EMEX9 trajectories (although the *sum* of the remaining six terms is about half as big as the buoyancy gradient term at the time of maximum upward pressure gradient forcing). Thus shear plays a secondary role to the vertical gradient of buoyancy here. Figure 6 shows that the vertical pressure gradient along each of these trajectories reaches a minimum (i.e., the upward-directed pressure gradient force is a maximum) just as the trajectories begin their ascent. Also, note in Figure 6 that the buoyancy increases to a maximum a little *after* the minimum in vertical pressure gradient. The particle is nearly neutrally buoyant at the time of the pressure gradient minimum, indicating that the ascent is dynamically forced, initially.

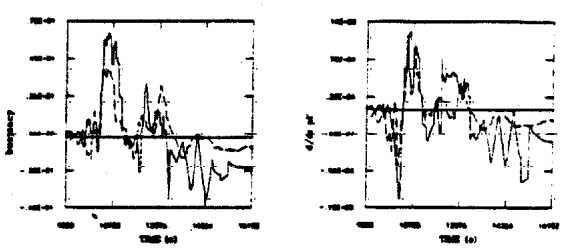

Figure 6. Values of (a) the buoyancy force (ms^{-2}) and (b) the vertical gradient of perturbation Exner function ($ms^{-2}K^{-1}$) along two front-to-rear system-relative trajectories. The solid (dashed) line is for the trajectory that ends up at 14 (6) km.

Conclusions

We have used RAMS to perform a three-dimensional simulation of the EMEX9 mesoscale convective system which was probed by research aircraft on 2-3 February 1987 during the Equatorial Mesoscale Experiment. RAMS successfully captures the observed characteristics of EMEX9, including temporal initiation, geographic location, speed and direction of motion of the system, spatial arrangement of the convective cells and stratiform region, and updraft and downdraft speeds.

We have used several different kinds of analysis techniques in order to distill the copious amounts of data provided by the simulation into some coherent view of EMEX9. Conditional sampling of model output uncovers a strange convergence maximum at about 10 km in the intermediary region—perhaps a physical footprint of the production of EMEX9's vast stratiform anvil. Applying the RAMS LPDM enables us to identify the major simulated flow branches, including a conspicuous front-to-rear ascending flow branch. Analysis of vertical forcing terms along this flowbranch shows that a brief burst of upward directed vertical pressure gradient force initiates the ascent before upward buoyancy dominates, consistent with the idea that some trigger is needed to force ascent into a conditionally unstable atmosphere.

Acknowledgments

This work was supported by the Department of Energy under grant numbers DE-FG02-90ER61066 and DE-FG03-94ER61749.

References

Barnes, S. L. 1973. Mesoscale objective map analysis using weighted time-series observations. NOAA Tech. Memo. ERL NSSL-62 [NTIS COM-73-10781], March, National Severe Storms Laboratory, Norman, Oklahoma, 60 pp.

Bograd, S. J. 1989. The mesoscale structure of precipitation in EMEX cloud clusters. M.S. thesis, University of Washington, 143 pp.

Mapes, B. E. 1992. The Australian monsoon and its mesoscale convective systems. Ph.D. dissertation, University of Washington.

Mapes, B. E. 1993. Gregarious tropical convection. *J. Atmos. Sci*. **50**:2026-2037.

Mapes, B., and R. A. Houze, Jr. 1992. An integrated view of the 1987 Australian monsoon and its mesoscale convective systems. I: Horizontal structure. *Quart. J. Roy. Meteor. Soc.* **118**:927-963.

Mapes, B., and R. A. Houze, Jr. 1993. An integrated view of the 1987 Australian monsoon and its mesoscale convective systems. II: Vertical structure. Quart. *J. Roy. Meteor. Soc*. **119**:733-754.

Tao, W.-K., J. Simpson, C.-H. Sui, B. Ferrier., S. Lang, J. Scala, M.-D. Chou, and K. Pickering. 1993. Heating, moisture, and water budgets of tropical and midlatitude squall lines: Comparisons and sensitivity to longwave radiation. *J. Atmos. Sci*. **50**:673-690.

Webster, P. J., and R.A. Houze, Jr. 1991. The Equatorial Mesoscale Experiment (EMEX): An overview. *Bull. Amer. Meteor. Soc.* **72**:1481-1505.

Weissbluth, M. J., and W. R. Cotton. 1993. The representation of convection in mesoscale models. Part I: Scheme fabrication and calibration. *J. Atmos. Sci*. **50**:3852-3872.

Wong, T., G. L. Stephens, P. W. Stackhouse, Jr., and F.P.J. Valero. 1993. The radiative budgets of a tropical mesoscale convective system during EMEX-STEP-AMEX Experiment. II: Model results. *J. Geophys. Res*. **98**:8695-8711.